
Computer Methods in Biomechanics and Biomedical Engineering

Publication details, including instructions for authors and subscription information:
http://www.tandfonline.com/loi/gcmb20

# A fully implicit finite element method for bidomain models of cardiac electrophysiology

Hüsnü Dal [a], Serdar Göktepe [b], Michael Kaliske [a] & Ellen Kuhl [c]

[a] Institute for Structural Analysis, Technische Universität Dresden, Dresden, D-01062, Germany

[b] Department of Civil Engineering, Division of Construction Materials, Middle East Technical University, Ankara, TR-06531, Turkey

[c] Departments of Mechanical Engineering, Bioengineering, and Cardiothoracic Surgery, Stanford University, Stanford, CA, 94305, USA

Available online: 24 May 2011

To cite this article: Hüsnü Dal, Serdar Göktepe, Michael Kaliske & Ellen Kuhl (2012): A fully implicit finite element method for bidomain models of cardiac electrophysiology, Computer Methods in Biomechanics and Biomedical Engineering, 15:6, 645-656

To link to this article: http://dx.doi.org/10.1080/10255842.2011.554410

*Computer Methods in Biomechanics and Biomedical Engineering*
Vol. 15, No. 6, June 2012, 645–656

Taylor & Francis
Taylor & Francis Group

# A fully implicit finite element method for bidomain models of cardiac electrophysiology

Hüsnü Dal[a]*, Serdar Göktepe[b], Michael Kaliske[a] and Ellen Kuhl[c]

[a]*Institute for Structural Analysis, Technische Universität Dresden, Dresden D-01062, Germany;* [b]*Department of Civil Engineering, Division of Construction Materials, Middle East Technical University, Ankara TR-06531, Turkey;* [c]*Departments of Mechanical Engineering, Bioengineering, and Cardiothoracic Surgery, Stanford University, Stanford CA 94305, USA*

(*Received 27 September 2010; final version received 10 January 2011*)

This work introduces a novel, unconditionally stable and fully coupled finite element method for the bidomain system of equations of cardiac electrophysiology. The transmembrane potential $\phi_i - \phi_e$ and the extracellular potential $\phi_e$ are treated as independent variables. To this end, the respective reaction-diffusion equations are recast into weak forms via a conventional isoparametric Galerkin approach. The resultant nonlinear set of residual equations is consistently linearised. The method results in a symmetric set of equations, which reduces the computational time significantly compared to the conventional solution algorithms. The proposed method is inherently modular and can be combined with phenomenological or ionic models across the cell membrane. The efficiency of the method and the comparison of its computational cost with respect to the simplified monodomain models are demonstrated through representative numerical examples.

**Keywords:** cardiac electrophysiology; finite element method; bidomain models; implicit methods



## 1. Introduction

Heart rhythm disorders, also known as arrhythmia, are the leading cause of death in developed countries. Cardiac arrhythmias can be debilitating and even life-threatening unless not treated. Although readily available artificial pacemakers and advent of implantable defibrillators revolutionised their treatment, the success of these devices can be further improved by feeding these devices with patient-specific data. Abnormal heart rhythms fall into two general categories: slow heart rates known as bradycardias, and rapid heart rates known as tachycardias. Among the most common tachycardias are fibrillations, which can occur either in the atria or in the ventricles. Atrial fibrillation occurs if the cardiac impulse fails to follow a regular circuit and divides along multiple pathways, a chaos of uncoordinated beats. Although atrial fibrillation may cause 20–30% reduction of the heart's pumping efficiency, the amount of blood pumped by the ventricles usually remains within the margins, because the atrioventricular node may block out many of the chaotic beats. In contrast to supraventricular arrhythmias, ventricular arrhythmias are potentially more serious and death can occur within 3–4 min. Prevention of the potentially dangerous contractions emerging from ventricular fibrillation is crucial, because only around one fourth of such patients recover and continue to lead normal lives. When ventricular fibrillation occurs, defibrillation, delivery of large electric shock to the heart, is an emergency measure, see Zaret et al. (1992). Despite tremendous scientific improvements during the past decades, the treatment of cardiac arrhythmias is mainly based on the personal experience of the individual cardiologist. Guidance through simulations based on patient-specific data can improve the treatment strategy tremendously. In order to optimise a medical treatment strategy, it is essential to understand the electrophysiology of the heart, in particular, the generation of the electrical re-entrant spiral and scroll waves and the mechanisms of successful and unsuccessful defibrillation. This necessitates the development of efficient numerical tools for the electrophysiology of the heart.

The goal of this work is to develop a robust and efficient computational framework for the bidomain model of electrophysiology that enables the simulation of electrical excitation of the heart and its response to an externally applied shock. At the cellular level, cardiac tissue is formed by intracellular space $\Omega_i$ and extracellular space $\Omega_e$, and the cell membrane $\Gamma$, where the ionic channels rest. Bidomain equations represent a homogenisation of the intracellular and extracellular medium, see Figure 1. They were first applied to cardiac tissue by Tung (1978) and Miller and Geselowitz (1978). For a given point of the continuum, intra- and extracellular spaces coexist and are separated by the continuous cellular membrane (Sachse 2004; Colli Franzone et al. 2006). The ion flow from one space to other through membrane is described by nonlinear phenomenological or ionic models, see Keener and Sneyd (1998). The solution of the

*Corresponding author. Email: huesnue.dal@tu-dresden.de

ISSN 1025-5842 print/ISSN 1476-8259 online

http://dx.doi.org/10.1080/10255842.2011.554410
http://www.tandfonline.com

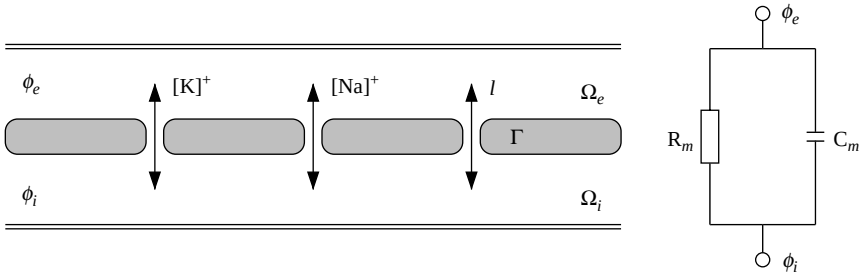


Figure 1. One-dimensional representation of myocardium and approximation of the cell membrane by resistor-capacitor circuit. The circuit consists of a nonlinear resistor $R_m$ dependent on the ionic concentrations (Sodium $[Na]^+$, Potassium $[K]^+$ and leakage currents) of intra- and extracellular domains and a capacitor $C_m$.



bidomain equations is quite complex due to the coupled representation of the reaction-diffusion equations which consist of parabolic and elliptic sub-problems. For the spatial discretisation of the model, the finite element method (Sundnes et al. 2005; Colli Franzone et al. 2006; Pathmanathan et al. 2010), the finite difference method (Pollard et al. 1992) and the finite volume method (Johnston 2010) were used. The degenerate parabolic form of the equations is found computationally expensive. This leads to the application of the simplified *monodomain model*, derived under the assumption of proportionality in between extra- and intracellular domains. The solution of the ordinary differential equations (ODEs) representing the electrophysiology of the cells accounts for the computationally most demanding part. Traditionally, the time integration of the equations is carried out with explicit methods such as Runge–Kutta method or forward Euler method, because their numerical derivation is straightforward and cheaper at first glance. This restricts the solution to very small time steps due to stability requirements and necessitates preconditioning algorithms which in turn lead to very demanding algorithmic issues, see Gerardo-Giorda et al. (2009) and dos Santos et al. (2004) and references therein. Efforts were made in order to overcome the drawbacks pertaining to the explicit methods. Within this context, Keener and Bogar (1998) proposed semi-implicit and Crank–Nicolson schemes for the solution of the ODEs. Skouibine et al. (2000) developed a predictor-corrector time stepping algorithm. Operator splitting is an alternative strategy for the solution of the bidomain equations. The partial differential Equations $(15)_1$ and $(15)_2$ describing the bidomain model can be split and solved iteratively. As a first step, $(15)_2$ is solved treating transmembrane potential $\phi$ constant, whereas the external potential $\phi_e$ is kept constant during solution $(15)_1$, see Vigmond et al. (2002, 2003). Outer iterations or three-step operator splitting is employed in order to improve the stability and accuracy of the operator splitting algorithms, see Vigmond et al. (2008) and references therein.

This article presents a fully implicit, monolithic Galerkin-type finite element method for the coupled bidomain model. Thereby, the transmembrane potential $\phi$ and extracellular potential $\phi_e$ are treated as global independent state variables. The local temporal evolution of the state variables and the global rate equations are integrated through unconditionally stable backward Euler scheme. The local and global iterations of the nonlinear residual equations are solved via the iterative Newton–Raphson algorithm. In order to describe the ion exchange across the cell membrane, the generic membrane model of Aliev and Panfilov (1996) is used. However, the extension of the approach to more sophisticated ionic membrane models is straightforward. The recovery variable of the membrane model, which is local in nature and keeps the history of the ion exchange between intra- and extracellular domain, is updated and stored locally at Gauss quadrature points. The developed FE scheme is applied to benchmark polarisation of a passive myocardium subjected to externally applied electric field and defibrillation of a spiral wave via an externally applied electric shock.

This work is organised as follows. Section 2 briefly summarises the bidomain model of cardiac electrophysiology and its monodomain reduction. Section 3 describes the fully implicit, monolithic finite element solution scheme for the bidomain equations. The weak form is established based on the Galerkin method. The resulting residual equations are consistently linearised and updated via Newton iteration scheme. Section 4 illustrates the proposed solution algorithm and addresses successful and unsuccessful defibrillation problems and relevant computational aspects. This work ends with final remarks in Section 5.

## 2. Bidomain models of cardiac electrophysiology

In this section, we introduce the fundamental equations of the coupled initial boundary value problem of bidomain cardiac electrophysiology. The *bidomain model* equations

are based on the homogenised geometrical description of the diffusion-reaction equations of extra- and intracellular media. Thereby, the *transmembrane potential* $\phi$, which is the unique field variable in the monodomain model, is defined as the difference between the intracellular potential $\phi_i$ and extracellular potential $\phi_e$ and it is also known as *action potential*. Contrary to the monodomain model, the intra- and extracellular potentials are treated as independent field variables in the coupled bidomain model. The electrophysiology of a material point $\mathbf{X}$ of cardiac tissue at time $\tau$ is defined as follow:

$$\text{State}(\mathbf{X}, \tau) := \{\phi_i(\mathbf{X}, \tau),\ \phi_e(\mathbf{X}, \tau)\}. \tag{1}$$

In the absence of externally applied current to a subdomain $\mathscr{P}$ of body $\mathscr{B}$, in the particular case, the human heart, the total current flux $\mathrm{q}_t$ of the body is preserved, leading to the following conservation law on the boundary of the subdomain $\partial\mathscr{P}$:

$$\int_{\partial\mathscr{P}} \mathbf{q}_t \cdot \mathbf{n}\, \mathrm{d}A = 0; \quad \mathbf{q}_t = \mathbf{q}_i + \mathbf{q}_e, \tag{2}$$

where $\mathbf{q}_i$, $\mathbf{q}_e$ and $\mathbf{n}$ are the intra- and extracellular current flux vectors and the surface normal vector, respectively. Applying the Gauss theorem and the localisation theorem successively, the local form of (2) reads

$$\operatorname{div} \mathbf{q}_t = 0. \tag{3}$$

The constitutive relations between the current fluxes and the potentials of the intra- and extracellular medium follow the Ohm's law

$$\mathbf{q}_i = -\mathbf{D}_i \nabla \phi_i; \quad \mathbf{q}_e = -\mathbf{D}_e \nabla \phi_e. \tag{4}$$

Here, $\mathbf{D}_i$ and $\mathbf{D}_e$ are the intra- and extracellular conductance tensors, respectively. Moreover, we define the transmembrane potential $\phi = \phi_i - \phi_e$ and the transmembrane current $i_T$ as the sum of ionic and capacitive currents from intracellular space into extracellular space such that

$$i_T = \chi(\mathcal{C}_m \dot{\phi} + \mathcal{I}_{\text{ion}}(\phi, r)) \quad \text{with} \quad \phi = \phi_i - \phi_e, \tag{5}$$

where $\chi$ denotes the aspect ratio of the membrane surface to volume in a periodic representative unit of cardiac tissue. $\mathcal{C}_m$ and $\mathcal{I}_{\text{ion}}$ are the membrane capacitance per unit area and current density flowing through the membrane ion channels, see Figure 1. The transmembrane current $i_T$ acts as a source term from intracellular medium to extracellular medium, which can be accounted for in the current conservation equations of each subspace as follows:

$$\operatorname{div} \mathbf{q}_i = -i_T; \quad \operatorname{div} \mathbf{q}_e = i_T. \tag{6}$$

Equations (3) and (6) constitute the strong form of the coupled *bidomain model* of cardiac electrophysiology. Summation of $(6)_1$ and $(6)_2$ leads to the conservation of total current. At this stage, we introduce the extracardiac volume $\mathscr{B}_0$ and the respective boundary $\partial\mathscr{B}_0$ surrounding the heart $\mathscr{B}$, the extracardiac potential $\phi_0$ and the corresponding flux vector $\mathbf{q}_0 = \mathbf{D}_0 \nabla \phi_0$, $\mathbf{D}_0$ denoting the extracardiac conductance. Then, boundary conditions at the interface $\partial\mathscr{B}$ can be rewritten as:

$$\mathbf{q}_t \cdot \mathbf{n} = \mathbf{q}_0 \cdot \mathbf{n} \ \text{ on } \ \partial\mathscr{B}. \tag{7}$$

The extracardiac medium possesses no transmembrane currents, and the set of transient diffusion equation takes the simple form

$$\operatorname{div} \mathbf{q}_0 = 0 \ \text{ in } \ \mathscr{B}_0. \tag{8}$$

Equation (7) states that the total current field $\mathbf{q}_t$ can continuously be discretised for intra- and extracardiac medium leading to the following boundary conditions:

$$\phi_0 = \bar{\phi}_0 \ \text{ on } \ \partial\mathscr{B}_0^{\phi} \ \text{ and } \ \mathbf{q}_t \cdot \mathbf{n} = i_{\text{app}} \ \text{ on } \ \partial\mathscr{B}_0^{q}, \tag{9}$$

where $i_{\text{app}}$ denotes the applied current at the boundary. In the absence of extracardiac domain, the boundary simply equals to $\partial\mathscr{B}_0 = \partial\mathscr{B}$. The second set of equations stemming from $(6)_1$ or $(6)_2$ is bounded to the myocardium leading to the boundary conditions

$$\phi_{i,e} = \bar{\phi}_{i,e} \ \text{ on } \ \partial\mathscr{B}_{\phi} \ \text{ and } \ \mathbf{q}_{i,e} \cdot \mathbf{n} = \bar{q}_{i,e} \ \text{ on } \ \partial\mathscr{B}_{q}. \tag{10}$$

### 2.1 Monodomain model of cardiac electrophysiology

The bidomain model can be reduced to the widely used *monodomain model* after some simplifications. By making use of the identities $(4)_1$, $(4)_2$ and exploiting $(2)_2$, we obtain

$$\nabla \phi_i = \mathbf{D}^{-1}(\mathbf{D}_e \nabla \phi - \mathbf{q}_t); \quad \mathbf{D} = \mathbf{D}_i + \mathbf{D}_e. \tag{11}$$

Insertion of the result obtained in $(11)_1$ into $(6)_1$ and making use of the identity (5), we end up with the local form of the reaction-diffusion equations in terms of the transmembrane potential

$$\begin{aligned} i_T &= \chi \mathcal{C}_m \dot{\phi} + \chi \mathcal{I}_{\text{ion}} \\ &= \operatorname{div}(\mathbf{D}_i \mathbf{D}^{-1} \mathbf{D}_e \nabla \phi) - \operatorname{div}(\mathbf{D}_i \mathbf{D}^{-1} \mathbf{q}_t). \end{aligned} \tag{12}$$

The second term on the right-hand side brings an extra contribution to the transmembrane current. From the conservation law of the total current flux (2), we have $\operatorname{div} \mathbf{q}_t = 0$. If the intra- and extracellular conductances are taken to be proportional, e.g. $\mathbf{D}_i = \alpha \mathbf{D}_e$ where $\alpha$ is a scalar quantity, then the second term on the right-hand side of

(12) vanishes, and the local form of the transient partial differential equation for the transmembrane potential reduces to

$$\chi \mathcal{C}_m \dot{\phi} + \chi \mathcal{I}_{\text{ion}}(\phi, r) = \text{div}(\hat{\mathbf{D}} \cdot \nabla \phi). \tag{13}$$

This is known as the *monodomain model*, where the effective monodomain conductance reads $\hat{\mathbf{D}} = \mathbf{D}_i(\mathbf{D}_i + \mathbf{D}_e)^{-1}\mathbf{D}_e$. Although the proportionality assumption simplifies the problem to a great extent, it is not justifiable from a physical point of view. This difference becomes apparent when the intracellular and extracellular polarisation and depolarisation patterns are examined during defibrillation of the heart by strong electric shock applied and commented by Trayanova (2006). For the sake of convenience, (13) is recast into a simple form

$$\dot{\phi} = \text{div}\, \hat{\mathbf{q}}(\phi) + f^{\phi}(\phi, r).$$

Here, the transmembrane current $\hat{\mathbf{q}} = \mathbf{D}_m \nabla \phi$, the effective monodomain conductance $\mathbf{D}_m = (\chi \mathcal{C}_m)^{-1}\hat{\mathbf{D}}$ and the ionic currents $f^{\phi}(\phi, r) = -\mathcal{I}_{\text{ion}}(\phi, r)/\mathcal{C}_m$ are defined, respectively.

## 3. Finite element implementation

In this section, we present a novel coupled finite element formulation for the bidomain model in terms of the transmembrane potential $\phi$ and the external potential $\phi_e$. We employ isoparametric shape functions for the spatial discretisation of these two field variables. The discrete set of residual equations is linearised and updated monolithically. The resulting solution algorithm is unconditionally stable and quadratically convergent when linearised consistently and solved with an incremental iterative Newton scheme. For the sake of convenience, the bidomain Equations $(6)_1$ and (3) are recast into a more coherent form

$$\begin{aligned} \dot{\phi} &= \text{div}(\mathbf{D}_i \cdot \nabla \phi) + \text{div}(\mathbf{D}_i \cdot \nabla \phi_e) + f^{\phi}(\phi, r), \\ 0 &= -\text{div}(\mathbf{D}_i \cdot \nabla \phi) - \text{div}(\mathbf{D} \cdot \nabla \phi_e) \end{aligned} \tag{15}$$

along with the normalised conductances $\mathbf{D} \leftarrow (\chi \mathcal{C}_m)^{-1}\mathbf{D}$ and $\mathbf{D}_i \leftarrow (\chi \mathcal{C}_m)^{-1}\mathbf{D}_i$. $(15)_1$ is a parabolic partial differential equation, whereas $(15)_2$ defines an elliptic partial differential equation.

### 3.1 Weak formulation based on the Galerkin method

In what follows, we apply the well-known Galerkin procedure to construct the weak form of the governing equations to be solved by the finite element method. To this end, the residual equations are multiplied by square-integrable weight functions $\delta\Phi = [\delta\phi, \ \delta\phi_e]^T$ that satisfy $\delta\Phi = \mathbf{0}$ on $\partial\mathscr{B}_{\phi}$. Firstly, the weighted residual equations are integrated over the volume. Then, integration by parts is applied leading to the weak forms

$$G^{\phi}(\delta\phi, \phi, \phi_e) = G^{\phi}_{\text{int}}(\delta\phi, \phi, \phi_e) - G^{\phi}_{\text{ext}}(\delta\phi) = 0 \tag{16}$$

for the transmembrane potential and

$$G^{\phi_e}(\delta\phi_e, \phi, \phi_e) = G^{\phi_e}_{\text{int}}(\delta\phi_e, \phi, \phi_e) - G^{\phi_e}_{\text{ext}}(\delta\phi_e) = 0 \tag{17}$$

for the external potential, respectively. In the above equations, the internal $G^{\phi}_{\text{int}}$ and the external $G^{\phi}_{\text{ext}}$ terms in (16) are defined as follows:

$$\begin{aligned} G^{\phi}_{\text{int}}(\delta\phi, \phi, \phi_e) &= \int_{\mathscr{B}} (\delta\phi\dot{\phi} + \nabla(\delta\phi) \cdot \mathbf{D}_i \cdot (\nabla\phi + \nabla\phi_e))\, \text{d}V \\ G^{\phi}_{\text{ext}}(\delta\phi) &= \int_{\mathscr{B}} \delta\phi f^{\phi}\, \text{d}V + \int_{\partial\mathscr{B}} \delta\phi\, \bar{q}_i\, \text{d}A, \end{aligned} \tag{18}$$

respectively. $\bar{q}_i = \mathbf{D}_i \cdot (\nabla\phi + \nabla\phi_e) \cdot \mathbf{n}$ describes the natural boundary condition. In a similar way, the internal $G^{\phi_e}_{\text{int}}$ and the external $G^{\phi_e}_{\text{ext}}$ terms in (17) read

$$\begin{aligned} G^{\phi_e}_{\text{int}}(\delta\phi_e, \phi, \phi_e) &= \int_{\mathscr{B}} \nabla(\delta\phi_e) \cdot (\mathbf{D} \cdot \nabla\phi_e + \mathbf{D}_i \cdot \nabla\phi)\, \text{d}V \\ G^{\phi_e}_{\text{ext}}(\delta\phi_e) &= \int_{\partial\mathscr{B}} \delta\phi_e\, \bar{q}_t\, \text{d}A, \end{aligned} \tag{19}$$

respectively. $\bar{q}_t = (\mathbf{D}_e \cdot \nabla\phi_e + \mathbf{D}_i \cdot \nabla\phi_i) \cdot \mathbf{n}$ is equal to the total current flux at the boundary. The nonlinear source term $f^{\phi}$ in $(18)_2$ brings an extra contribution to the tangent term of the linearised residual expression. At this stage, we define the incremental time frame $\Delta\mathcal{T} := [\tau_n, \ \tau_n + \Delta\tau]$ where $\tau$, $\tau_n$ and $\Delta\tau = \tau - \tau_n$ are the current time step, previous time step and the time increment, respectively. The time derivative of the transmembrane potential is approximated by the backward Euler scheme

$$\dot{\phi} \approx \frac{\phi - \phi_n}{\Delta\tau}; \quad \phi_n := \phi(\mathbf{X}, \tau_n). \tag{20}$$

### 3.2 Consistent algorithmic linearisation

The weak forms of the residual Equations $(15)_1$ and $(15)_2$ are nonlinear functions of the field variable $\phi$ due to the nonlinear dependence of the constitutive functions $f^{\phi}(\phi, r)$ and $\dot{r} = f^{r}(\phi, r)$. Thereby, the Newton-type iterative solution schemes will be applied within the framework of the implicit finite element method. Consistent linearisations of (16) and (17) around a

non-equilibrium intermediate step $\tilde{\phi}$ and $\tilde{\phi}_e$ read

$$\begin{aligned}\mathrm{Lin}\, G^{\phi}(\delta\phi,\tilde{\phi},\tilde{\phi}_e) &:= G^{\phi}(\delta\phi,\tilde{\phi},\tilde{\phi}_e)\\ &\quad + \Delta G^{\phi}(\delta\phi,\tilde{\phi},\tilde{\phi}_e;\Delta\phi,\Delta\phi_e),\\ \mathrm{Lin}\, G^{\phi_e}(\delta\phi_e,\tilde{\phi},\tilde{\phi}_e) &:= G^{\phi_e}(\delta\phi_e,\tilde{\phi},\tilde{\phi}_e)\\ &\quad + \Delta G^{\phi_e}(\delta\phi,\tilde{\phi},\tilde{\phi}_e;\Delta\phi,\Delta\phi_e).\end{aligned} \tag{21}$$

The incremental terms $\Delta G^{\phi}$ and $\Delta G^{\phi_e}$ are expressed as

$$\Delta G^{\gamma} = \Delta G^{\gamma}_{\mathrm{int}} - \Delta G^{\gamma}_{\mathrm{ext}} \quad \text{for} \quad \gamma = \phi, \phi_e. \tag{22}$$

The derivation of the incremental terms $\Delta G^{\phi}_{\mathrm{int}}$ and $\Delta G^{\phi}_{\mathrm{ext}}$ of the first residual term is carried out as follows:

$$\begin{aligned}\Delta G^{\phi}_{\mathrm{int}} &= \int_{\mathscr{B}} \delta\phi \frac{\Delta\phi}{\Delta\tau}\,\mathrm{d}V + \int_{\mathscr{B}} \nabla(\delta\phi)\cdot\mathbf{D}_i\cdot\nabla(\Delta\phi+\Delta\phi_e)\,\mathrm{d}V,\\ \Delta G^{\phi}_{\mathrm{ext}} &= \int_{\mathscr{B}} \delta\phi H \Delta\phi \quad \text{with} \quad H := \frac{\mathrm{d}f^{\phi}(\phi,r)}{\mathrm{d}\phi}.\end{aligned} \tag{23}$$

Similarly, the incremental term in $(21)_2$ takes the simple form

$$\begin{aligned}\Delta G^{\phi_e}_{\mathrm{int}} &= \int_{\mathscr{B}} \nabla(\delta\phi_e)\cdot\mathrm{D}\cdot\nabla(\Delta\phi_e)\,\mathrm{d}V + \int_{\mathscr{B}} \nabla(\delta\phi_e)\cdot\mathrm{D}_i\cdot\nabla(\Delta\phi)\,\mathrm{d}V,\\ \Delta G^{\phi_e}_{\mathrm{ext}} &= 0.\end{aligned} \tag{24}$$

### 3.3 Spatial discretisation

The temporal discretisation of the weak form (16) is given in Section 3.1. The spatial discretisation of the weak forms (16) and (17) is achieved via a conventional isoparametric Galerkin procedure. To this end, domain $\mathscr{B}$ is divided into subdomains $\mathscr{B} = \cup_{e=1}^{n_{\mathrm{el}}} \mathscr{B}^e$ with $n_{\mathrm{el}}$ being the number of the subdomains $\mathscr{B}^e$, which are in the context of finite element method, corresponding to element domain $\mathscr{B}^h = \mathscr{B}^e$. The field equations are approximated over the element domain via $\mathcal{C}^0$ shape functions

$$\begin{aligned}\delta\phi &= \sum_{a=1}^{n_{en}} N^a \delta\Phi^h_a; \quad \delta\phi_e = \sum_{a=1}^{n_{en}} N^a \delta\Phi^h_{e_a},\\ \phi &= \sum_{a=1}^{n_{en}} N^a \Phi^h_a; \quad \phi_e = \sum_{a=1}^{n_{en}} N^a \Phi^h_{e_a},\end{aligned} \tag{25}$$

where $N^a(\mathbf{X})$ and $n_{\mathrm{en}}$ refer to the shape functions and the number of nodes per element, respectively. $\Phi^h_a$ and $\Phi^h_{e_a}$ denote the discrete nodal values of the field variables. Based on (25), the spatial gradients read as follows:

$$\begin{aligned}\nabla(\delta\phi) &= \sum_{a=1}^{n_{en}} \delta\Phi^h_a \otimes \nabla N^a,\\ \nabla(\delta\phi_e) &= \sum_{a=1}^{n_{en}} \delta\Phi^h_{e_a} \otimes \nabla N^a.\end{aligned} \tag{26}$$

Likewise, the spatial gradients of the incremental fields are obtained as follows

$$\begin{aligned}\nabla(\Delta\phi) &= \sum_{a=1}^{n_{\mathrm{en}}} \Delta\Phi^h_a \otimes \nabla N^a,\\ \nabla(\Delta\phi_e) &= \sum_{a=1}^{n_{\mathrm{en}}} \Delta\Phi^h_{e_a} \otimes \nabla N^a.\end{aligned} \tag{27}$$

Incorporating the results (25), (26) into (16), (17) along with (18) and (19), we end up with the discrete residual vectors

$$\begin{aligned}\mathbf{R}^{\phi} &= \mathop{\mathsf{A}}_{e=1}^{n_{\mathrm{el}}} \left\{ \int_{\mathscr{B}^e} \left[ N^a \frac{\phi-\phi_n}{\Delta\tau} + \nabla N^a_b \left( D^{bc}_i \nabla\phi_c + D^{bc}_i \nabla\phi_{e_c} \right) \right] \mathrm{d}V \right.\\ &\quad \left. - \int_{\mathscr{B}^e} N^a f^{\phi}\,\mathrm{d}V - \int_{\partial\mathscr{B}^e} N^a \bar{q}_i\,\mathrm{d}A \right\},\\ \mathbf{R}^{\phi_e} &= \mathop{\mathsf{A}}_{e=1}^{n_{\mathrm{el}}} \left\{ \int_{\mathscr{B}^e} \left[ \nabla N^a_b \left( D^{bc} \nabla\phi_{e_c} + D^{bc}_i \nabla\phi_c \right) \right] \mathrm{d}V \right.\\ &\quad \left. - \int_{\partial\mathscr{B}^e} N^a \bar{q}_t\,\mathrm{d}A \right\}.\end{aligned} \tag{28}$$

The symbol $\mathsf{A}$ stands for the global assembly of the element quantities, whereas $I = 1, \ldots, n_{en}$ corresponds to the discrete $I$th nodal value of the element residual vector. Linearisation of $(28)_1$ and $(28)_2$ leads to

$$\begin{aligned}\mathrm{Lin}\,\mathsf{R} &= \mathsf{R} + \frac{\partial \mathsf{R}}{\partial\hat{\Phi}}\Delta\hat{\Phi}; \quad \mathsf{R} = \left\{ \begin{array}{c} \mathbf{R}^{\phi} \\ \mathbf{R}^{\phi_e} \end{array} \right\};\\ \Delta\hat{\Phi} &= \left\{ \begin{array}{c} \Phi^h_i \\ \Phi^h_e \end{array} \right\}.\end{aligned} \tag{29}$$

The coupled element matrix is derived via the incorporation of (25)–(27) into (23) and (24)

$$\mathsf{K} = \frac{\partial \mathsf{R}}{\partial\hat{\Phi}} = \mathop{\mathsf{A}}_{e=1}^{n_{\mathrm{el}}} \mathsf{K}_{\mathsf{el}}; \quad \mathsf{K}_{\mathsf{el}} := \begin{bmatrix} \mathsf{A}_{\mathsf{i}} + \mathsf{C} & \mathsf{A}_{\mathsf{i}} \\ \mathsf{A}_{\mathsf{i}} & \mathsf{A} \end{bmatrix}, \tag{30}$$

where the components of element matrix $\mathsf{K}_{\mathsf{el}}$ are defined

as follows:

$$\begin{aligned}\mathsf{A}_{\mathrm{i}}^{ab} &= \int_{\mathscr{B}^e} \nabla N_c^a D_i^{cd} \nabla N_b^d \,\mathrm{d}V,\\ \mathsf{A}^{ab} &= \int_{\mathscr{B}^e} \nabla N_c^a D^{cd} \nabla N_b^d \,\mathrm{d}V,\\ \mathsf{C}^{ab} &= \int_{\mathscr{B}^e} N^a \left(\frac{1}{\Delta\tau} - H\right) N^b \,\mathrm{d}V.\end{aligned} \tag{31}$$

The crucial point in the formulation is the consistent linearisation $H$

$$H := \frac{\mathrm{d}f^{\phi}(\phi, r)}{\mathrm{d}\phi} = \partial_{\phi} f^{\phi} + \partial_r f^{\phi} d_{\phi} r \tag{32}$$

of constitutive function $f^{\phi}$ which renders the time integration of ODE at hand fully implicit. Pathmanathan et al. (2010) have recently proposed a coupled solution algorithm based on the semi-implicit time integration method where the linearisation $\subset^{ab}$ $(31)_3$ only considers the implicit update of the term $[\phi - \phi_n]/\Delta\tau$. They report that *the fully implicit discretisation of $f^{\phi}$ term in time requires the solution of a massive nonlinear system, with size given by the product of the nodes in the computational mesh and the number of dependent variables included in* (5) *and* (6). However, in the formulation proposed in this contribution, the number of equations and unknowns is exactly equivalent to the scheme proposed by Pathmanathan et al. (2010). The essential point in the time integration is to keep the recovery variable $r_n$ as a history variable at Gauss quadrature points similar to the internal variable formulations in viscoelasticity and elastoplasticity, because these variables are local in nature. We refer to Göktepe and Kuhl (2009), Kotikanyadanam et al. (2010) and Göktepe et al. (2010) for the further details on the consistent total derivative of the constitutive term $f^{\phi}$. The iterative update for the increments of the global unknowns $\hat{\Phi}$ at an iteration step $k+1$ follows straightforwardly

$$\hat{\Phi}^{k+1} \leftarrow \hat{\Phi}^k + \Delta\hat{\Phi}^{k+1}; \quad \Delta\hat{\Phi}^{k+1} = -\mathsf{K}^{-1} \cdot \mathsf{R}^k, \tag{33}$$

until a certain convergence criterion $|\mathsf{R}| < \texttt{tol}$ is achieved.

## 4. Examples

This section is devoted to the representative 2D-dimensional numerical examples of cardiac tissue polarisation due to an externally applied electric field and a qualitative model example depicting defibrillation of a single re-entrant spiral wave. The re-entrant waves occur due to a variety of physiological origins and lead to fibrillatory states that compromise the heart's ability to contract and pump properly. Despite its importance, the initiation and termination of spiral and scroll waves are quite complex due to the challenges pertaining to the electrophysiology and geometry of the heart. In order to give insight into initiation, propagation and termination via an externally applied electric field and to validate the performance of the proposed finite element scheme, we analyse two benchmark examples on a simplified geometry.

### 4.1 Polarisation pattern due to externally applied electric field

We apply the numerical algorithm presented in Section 3 in order to compute the polarisation patterns developed due to non-proportional intra- and extracellular conductances as a benchmark. We choose a specific form of the intra- and extracellular conductances $\mathbf{D}_i := d^i_{\parallel}\mathbf{f}\otimes\mathbf{f} + d^i_{\perp}(\mathbf{I} - \mathbf{f}\otimes\mathbf{f})$ and $\mathbf{D}_e := d^e_{\parallel}\mathbf{f}\otimes\mathbf{f} + d^e_{\perp}(\mathbf{I} - \mathbf{f}\otimes\mathbf{f})$, respectively. $\mathbf{f}$ denotes the fibre orientation vector. $d^i_{\perp}$, $d^e_{\perp}$ and $d^i_{\parallel}$, $d^e_{\parallel}$ denote the conductances of intra- and extracellular domains along the fibre direction and the orthogonal plane to it, respectively. To this end, we select a square sheet of myocardium with analytically well-defined curving fibre geometries. This example was originally developed by Roth and Beaudoin (2003). They have proposed approximate analytical solutions for studying the polarisation patterns of passive heart tissue exposed to an externally applied electric field. A $20 \times 20$-mm$^2$ sheet of unit thickness with two different fibre orientation angles

$$\begin{aligned}\theta(x,y) &= -\sin\left(2\pi\frac{x}{20}\right)\sin\left(2\pi\frac{y}{20}\right),\\ \theta(x,y) &= -\cos^2\left(\pi\frac{x}{20}\right)\cos^2\left(\pi\frac{y}{20}\right)\end{aligned} \tag{34}$$

is considered. The in-plane orientation vector reads $\mathbf{f} := [\cos\theta \sin\theta 0]^T$. The origin of the square plate is taken at the centre. The two fibre orientations are analysed for horizontally and vertically applied electric fields obtained by assigning $\phi_e = \pm 5$ V at $x = \pm 10$ mm and $y = \pm 10$ mm, respectively. For this special case, the simplifications $\phi(t=0) = 0$, $\Delta\tau = 1$ ms and $\dot{\phi} \approx \phi$ are made in order to compute the initial polarisation pattern of the tissue as described by Roth and Beaudoin (2003). The tissue conductances are taken as $d^i_{\parallel} = 0.1863 \times 10^{-3}$ S/mm, $d^i_{\perp} = 0.186 \times 10^{-3}$ S/mm, $d^e_{\parallel} = 0.1863 \times 10^{-3}$ S/mm, $d^e_{\perp} = 0.745 \times 10^{-4}$ S/mm and normalised with $\chi C_m = 4.95 \times 10^{-4}$ S s/mm$^3$. The polarisation patterns corresponding to the fibre orientation $(34)_1$ are depicted in Figure 2(a,b), whereas Figure 2(c,d) corresponds to the fibre orientation $(34)_2$. The first row depicts the transmembrane potential $\phi$ at the onset of the externally applied electric field. The columns (a) and (c) are subjected to a vertically applied electric field, whereas

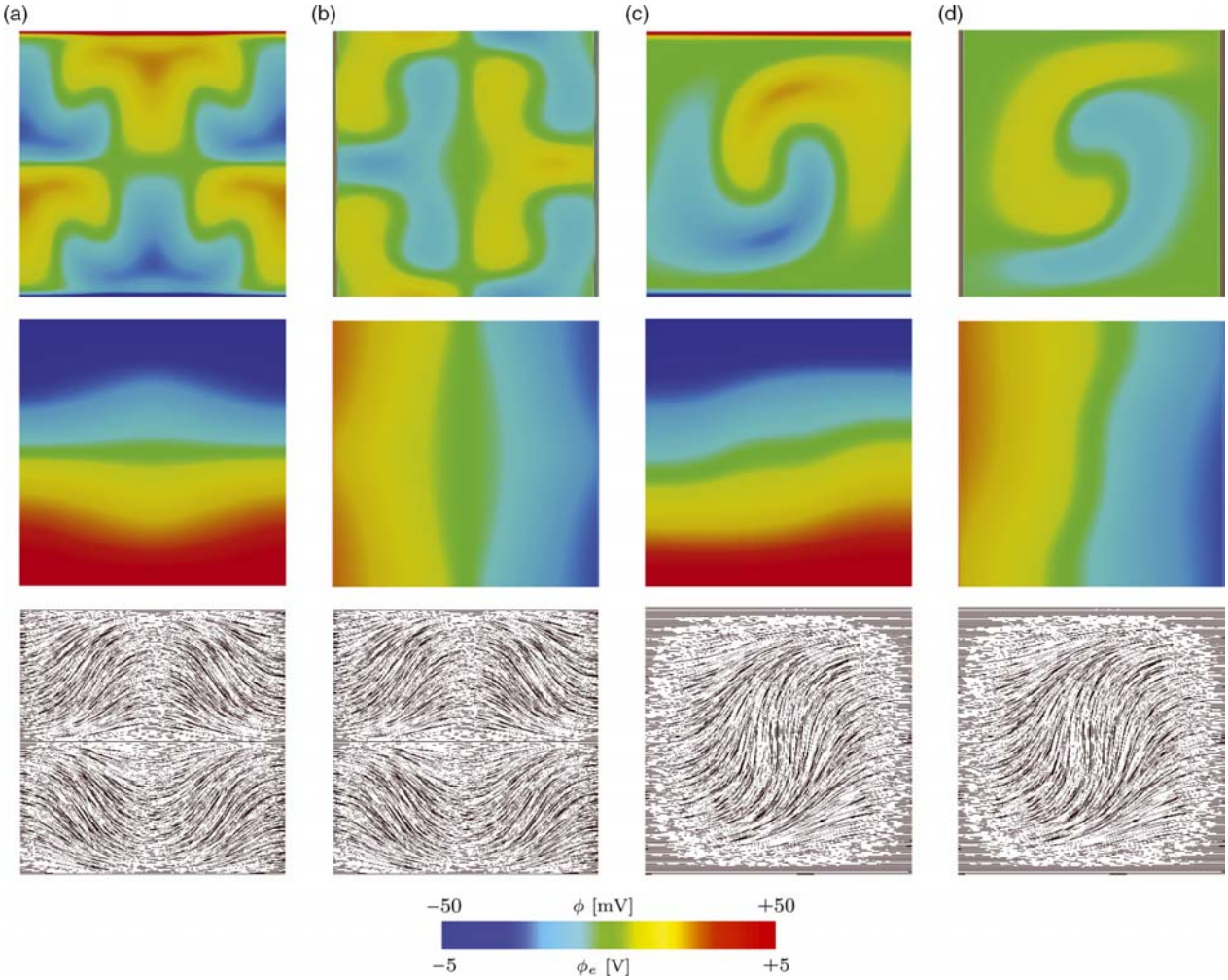


Figure 2. Instantaneous passive response of myocardium to an externally applied electric field $E = 500$ V/m for different analytically defined fibre orientations. The first, second and third rows depict the transmembrane potential $\phi$, the extracellular potential $\phi_e$ and the fibre orientation direction $\mathbf{f}$, respectively. The electrical field is applied in the vertical direction for (a) and (c) and horizontal directions for (b) and (d). The example is taken from Roth and Beaudoin (2003).

columns (b) and (d) are subjected to a horizontally applied electric field. The gradual shift in the extracellular potential $\phi_e$ in the direction of the applied electric field can be seen in the second row. The polarisation patterns observed in the first row are particularly interesting, because this effect can only be captured for unequal anisotropy ratios of extracellular and intracellular conductances and vanishes for $d^i_{\parallel}/d^e_{\parallel} = d^i_{\perp}/d^e_{\perp}$.

The results obtained comply with those shown by Roth and Beaudoin (2003). However, the results of Roth and Beaudoin only capture an equivalent static analysis of the coupled bidomain equation at the onset of the polarisation. In order to show the generality of the developed algorithm, the transient solution of the problem is obtained and depicted in Figure 3. The parameters used are identical to those in Figure 2. The time increment is gradually varied from $\Delta\tau = 0.2$ to 50 ms. The snapshots depicting the transient state of the solution in Figure 3 are taken at times $\tau = 0.2$, 1, 2, 4, 20, 100 and 5000 ms, respectively. The fibre orientations and the direction of the externally applied electric field are identical to those given in Figure 2. The convergence of the fully coupled transient system for this particular case is obtained in one step, independent of the step size $\Delta\tau$, because the source term $f^{\phi}$ is excluded during the analysis of the passive response of the tissue to externally applied electric field.

### *4.2 Defibrillation of a spiral wave through externally applied electric field*

In order to test the fully coupled formulation, the active response of the tissue should be taken into account by considering the ionic currents through the membrane. In what follows, the simulation of the generation and termination of a spiral wave through an external stimulus

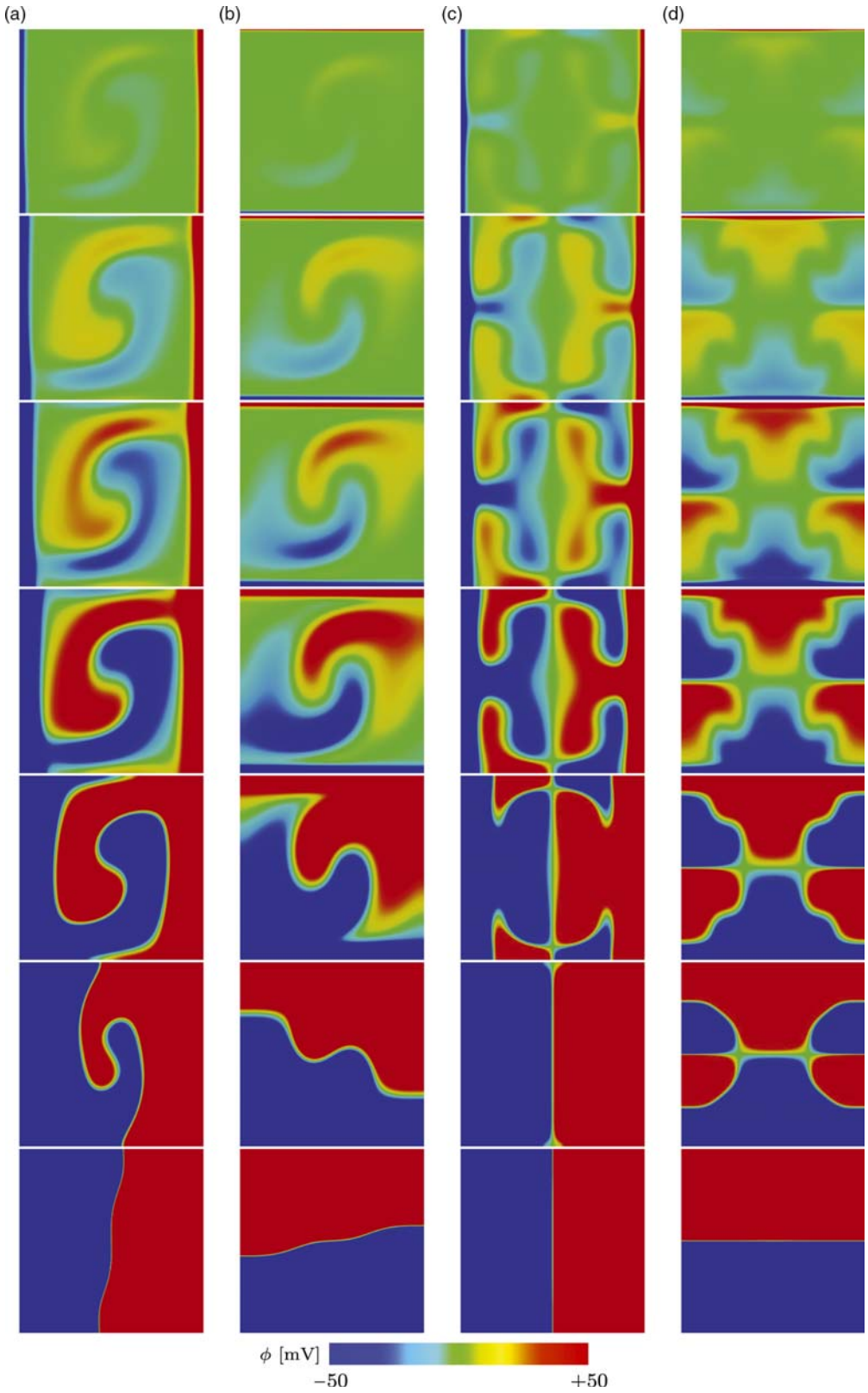


Figure 3. Transient passive response of myocardium to an externally applied electric field $E = 500$ V/m for different analytically defined fibre orientations. The transmembrane potential $\phi$ is depicted in columns (a)–(d) for the fibre orientations and the electric fields identical to those given in Figure 2, respectively.

injected into the extracellular medium is demonstrated. Aliev–Panfilov model will be used for the description of the transmembrane ionic currents. We consider a $100 \times 100$-mm$^2$ sheet of ventricular cardiomyocytes with fibre orientation

$$\theta(x, y) = -\cos^2\left(\pi \frac{x}{100}\right) \cos^2\left(\pi \frac{y}{100}\right), \qquad (35)$$

where the origin is located at the centre of the square domain. The details of the Aliev–Panfilov model and the derivation of the consistent time integration scheme suitable for the implicit finite element method were shown by Göktepe and Kuhl (2009) and Göktepe et al. (2010). The conversion of the non-dimensional action potential $\hat{\phi}$ and time $t$ in Aliev–Panfilov model to their physiological counterparts $\phi$ mV and $\tau$ ms is carried out through $\phi = 100\ \hat{\phi} - 80$ mV and $\tau = 12.9\ t$ ms. No conversion is required for the extracellular domain. The material parameters of the Aliev–Panfilov model are taken as $\alpha = 0.01$, $\gamma = 0.002$, $b = 0.15$, $c = 8$, $\mu_1 = 0.2$ and $\mu_2 = 0.3$. In order to initiate a planar wave, the initial values are set to $\phi_0 = -40$ mV at $x = -50$ mm and $\phi_0 = -80$ mV is considered for the rest of the myocardium sheet. The normalised conductances of the intra- and extracellular domains are taken as $d^i_{\parallel} = 0.5\,\text{mm}^2/\text{s}$, $d^i_{\perp} = 0.05\,\text{mm}^2/\text{s}$, $d^e_{\parallel} = 1.5\,\text{mm}^2/\text{s}$ and $d^e_{\perp} = 0.45 \times 10^{-4}\,\text{mm}^2/\text{s}$, respectively.

The square domain is discretised by $100 \times 100$ four-node isoparametric quadrilateral elements. In a stable resting tissue, two stimuli are applied in order to initiate a re-entrant wave pattern. The first stimulus is required to initiate a spatial gradient of recovery, whereas the second stimulus consists of a simple single excitation in repolarising the wave tail. In order to initiate a spiral wave, the second stimulus is given as an additional source term $f^{\phi} = 100$ in a region bounded by the coordinates

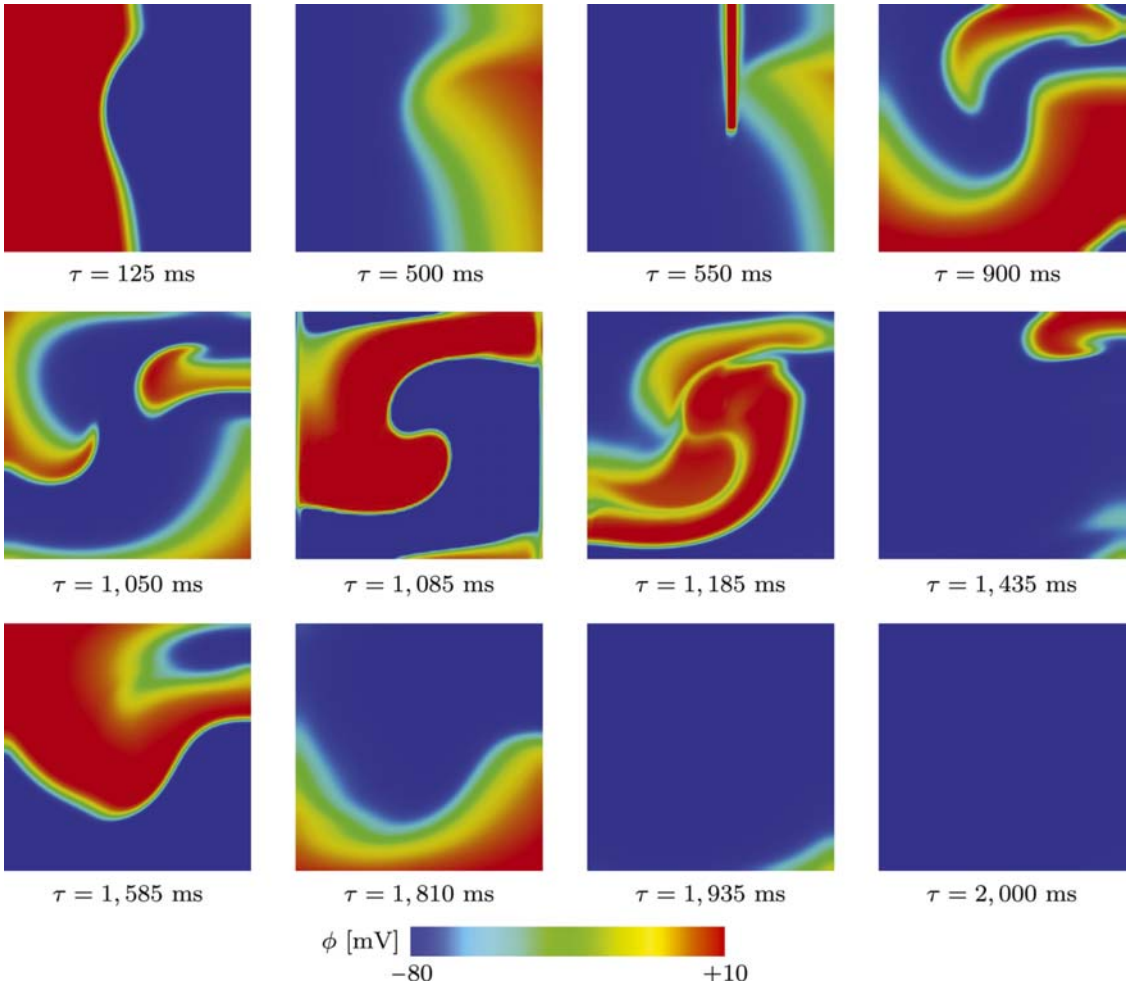


Figure 4. Successful defibrillation of a single spiral wave re-entry in square block of cardiac muscle tissue. Initiation of planar wave through initial excitation of $\phi_0 = -40$ mV at time $\tau = 0$ ms on the left boundary. Initiation of spiral wave through external stimulation of $f^{\phi}_{\text{stim}} = 100$ at time $\tau = 550$ ms for $\Delta t = 10$ ms. An external shock is applied at time $\tau = 1050$ ms for $\Delta t = 35$ ms in terms of influx $(\mathbf{q}_i + \mathbf{q}_e)\cdot\mathbf{n} = -1$ V mm/s at $x = 0$ and outflux $(\mathbf{q}_i + \mathbf{q}_e)\cdot\mathbf{n} = 1$ V mm/s at $x = 100$.

$x \in [17, 20]$ and $y \in [0, 50]$, origin taken at the centre of the domain. The timing and location of the second stimulus are crucial for the initiation of the spiral wave. The stimulus should fall in the vulnerability period in order to initiate a self-sustained re-entrant pattern of activation that continuously re-excites itself in an uncontrolled rate. The vulnerability period is controlled by the spatial gradient of excitability or $[Na]^+$ channel availability. The steeper gradient of excitability leads to shorter vulnerability period; in a particular model, this can be realised by the gradient of the recovery variable. Figure 4 clearly demonstrates the initiation and development of a spiral wave at time interval $\tau \in [0, 900]$, externally applied electric shock at time interval $\tau \in [1050, 1085]$, development of a meandering spiral wave at time $\tau = 1435$ and the successful defibrillation of the myocardium sheet at time $\tau = 2000$ ms, respectively. The external shock duration $\Delta\tau = 35$ ms and the injected current $(\mathbf{q}_i + \mathbf{q}_e)\cdot\mathbf{n} = 1$ V mm/s are selected for demonstrative purposes. The convergence of the algorithm is quadratic until the residual threshold and it is independent of the time step $\Delta\tau$. For this particular problem, time step is taken as $\Delta\tau = 5$ ms except during the externally applied shock where time step $\Delta\tau = 0.5$ ms at time interval $\tau \in [1050, 1085]$ ms is considered. No preconditioning is applied to the solution of global set of Equation (33). The convergence of the global problem is quadratic, and the relative residual tolerance $10^{-10}$ is reached within 3–7 iterations. During the delivery of the shock, convergence of the global problem turns linear due to the convergence problems during the internal iteration of the recovery variable in the Aliev–Panfilov model. After the release of the shock, convergence renders quadratic again.

The success of the defibrillation is controlled by several parameters. These are the polarity of the applied electrical shock, the duration of the shock and the

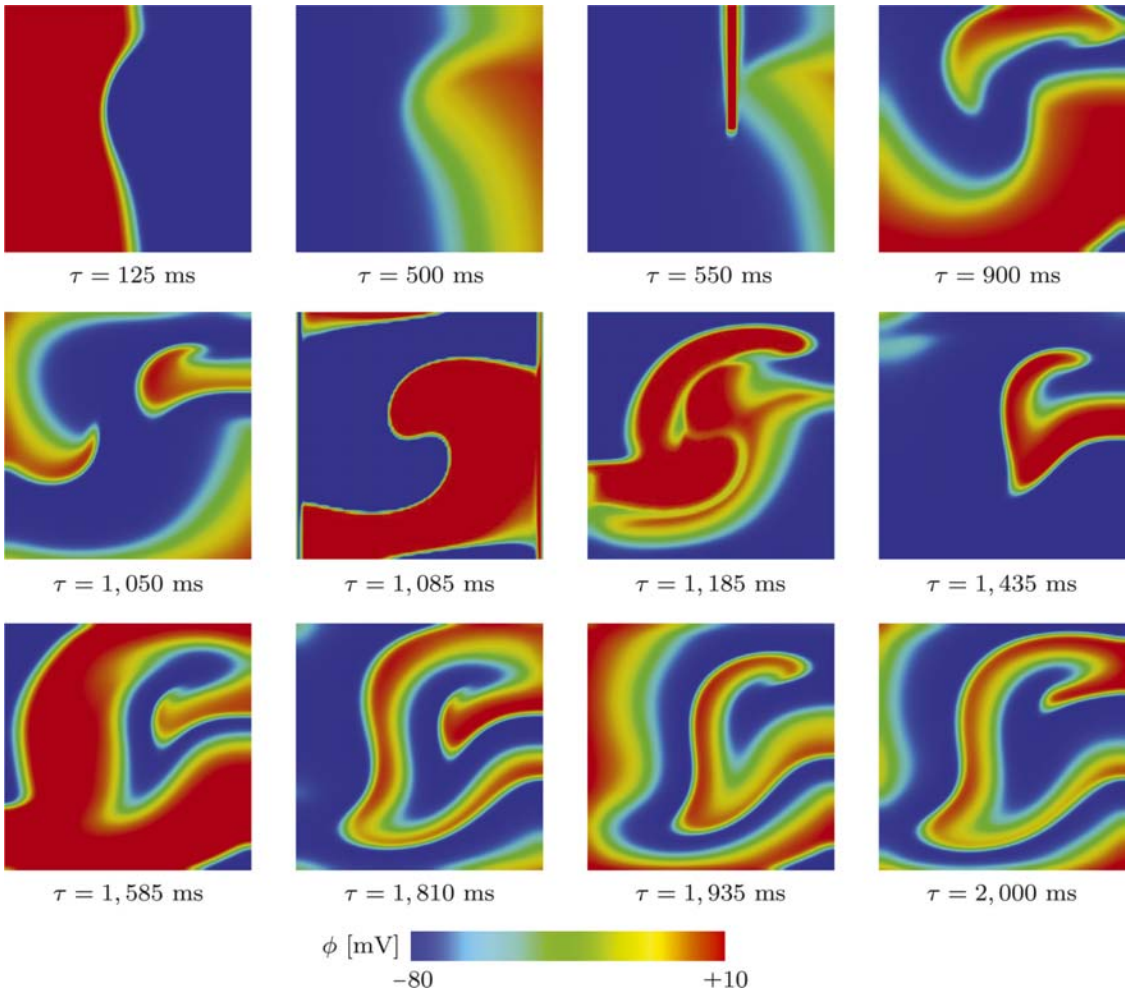


Figure 5. Unsuccessful defibrillation of a single spiral wave re-entry in square block of cardiac muscle tissue. Initiation of planar wave through initial excitation of $\phi_0 = -40$ mV at time $\tau = 0$ ms on the left boundary. Initiation of spiral wave through external stimulation of $f^{\phi}_{\text{stim}} = 100$ at time $\tau = 550$ ms for $\Delta t = 10$ ms. An external shock is applied at time $\tau = 1050$ ms for $\Delta t = 35$ ms in terms of outflux $(\mathbf{q}_i + \mathbf{q}_e)\cdot\mathbf{n} = 1$ V mm/s at $x = 0$ and influx $(\mathbf{q}_i + \mathbf{q}_e)\cdot\mathbf{n} = -1$ V mm/s at $x = 100$.

timing. Sometimes, the shock itself can generate self-sustained, re-entrant waves. In order to address the effect of the polarity, the previous problem is repeated by reversing the electric field by taking the influx $(\mathbf{q}_i + \mathbf{q}_e)\cdot\mathbf{n} = -1\,\mathrm{V\,mm/s}$. The results are depicted in Figure 5. Although the shock diminished the existing spiral waves successfully, at the end of the shock delivery $\tau = 1085\,\mathrm{ms}$, a new re-entry wavefront forms at the boundary of the hyperpolarised and depolarised regions due to the shock itself, because this zone falls in the vulnerable window at the timecourse of the applied shock. We refer to Trayanova (2001, 2006) and references therein for further discussions on the subject.

## 5. Concluding remarks

Understanding the electrophysiology of the heart is a challenging problem. The cardiac rhythm disorders, called arrhythmias, pose one of the paradoxes. Chronic and distressing arrhythmias, e.g. atrial tachycardia, atrial fibrillation and ventricular tachycardia, are treated with electrical cardioversion. To this end, the patient is given a short-acting intravenous anaesthetic, and an electrical shock is delivered from the defibrillator device through the conducting paddles applied to the chest. Hence, the shock delivered to the heart temporarily resets the electrical activity and lets the heart re-establish a normal rhythm. When ventricular fibrillation starts, electrical defibrillation is an emergency measure. The amount of the shock and the duration depends on the situation. Simulation of defibrillation is a challenging task and cannot be achieved by monodomain models, because the external stimulus is delivered to the system via the extracellular domain and causes polarisation of the tissue due to different conductances in the intra- and extracellular medium. Efficient numerical algorithms are crucial for the assistance of the clinical research. In this contribution, an efficient, fully implicit, unconditionally stable algorithm is presented for the solution of the coupled parabolic-elliptic set of equations of the bidomain model of cardiac electrophysiology. The algorithm is based on the discretisation of the extracellular potential $\phi_e$ and the transmembrane potential $\phi$ as global unknowns, whereas the recovery variable $r$ is treated as a local variable at Gauss point. Hence, the total number of unknowns is exactly the same as in the procedures utilising explicit or semi-implicit time discretisation. The developed procedure does not necessitate any further preconditioning techniques or similar algorithmic treatment of the ill-conditioned problem. The resulting global residual equations are quadratically convergent and unconditionally stable. This fact leads to significant reduction in computation time and enables larger time steps to be used compared to the existing procedures. The proposed finite element scheme is used for the demonstration of the instantaneous and transient polarisation patterns in a passive myocardium sheets with curved fibre orientations. Analysis of successful and unsuccessful defibrillation of a spiral wave is carried out for an active myocardium sheet, where the transmembrane currents are modelled with the Aliev–Panfilov model.



## References


Aliev RR, Panfilov AV. 1996. A simple two-variable model of cardiac excitation. Chaos, Solitons, Fractals. 7(3):293–301.

Colli Franzone P, Pavarino LF, Savaré G. 2006. Computational electrocardiology: mathematical and numerical modeling. In: Quarteroni A, Formaggia L, Veneziani A, editors. Complex systems in biomedicine. Milan: Springer. p. 187–241.

dos Santos R, Plank G, Bauer S, Vigmond E. 2004. Parallel multigrid preconditioner for the cardiac bidomain model. Biomed Eng IEEE Trans. 51:1960–1968.

Gerardo-Giorda L, Mirabella L, Nobile F, Perego M, Veneziani A. 2009. A model-based block-triangular preconditioner for the bidomain system in electrocardiology. J Comput Phys. 228:3625–3639.

Göktepe S, Kuhl E. 2009. Computational modeling of cardiac electrophysiology: a novel finite element approach. Int J Numer Methods Eng. 79:156–178.

Göktepe S, Wong J, Kuhl E. 2010. Atrial and ventricular fibrillation – computational simulation of spiral waves in cardiac tissue. Arch Appl Mech. 80:569–580.

Johnston PR. 2010. A finite volume method solution for the bidomain equations and their application to modelling cardiac ischaemia. Comput Methods Biomech Biomed Eng. 13:157–170.

Keener JP, Bogar K. 1998. A numerical method for the solution of the bidomain equations in cardiac tissue. Chaos: Interdisciplinary J Nonlinear Sci. 8:234–241.

Keener JP, Sneyd J. 1998. Mathematical physiology. New York: Springer.

Kotikanyadanam M, Göktepe S, Kuhl E. 2010. Computational modeling of electrocardiograms: a finite element approach towards cardiac excitation. Commun Numer Methods Eng. 26:524–533.

Miller WT, Geselowitz DB. 1978. Simulation studies of the electrocardiogram i: the normal heart. Circ Res. 43:301–315.

Pathmanathan P, Bernabeu MO, Bordas R, Cooper J, Garny A, Pitt-Francis JM, Whiteley JP, Gavaghan DJ. 2010. A numerical guide to the solution of the bidomain equations of cardiac electrophysiology. Progress Biophys Mol Biol. 102:136–155.

Pollard AE, Hooke N, Henriquez CS. 1992. Cardiac propagation simulation. Crit Rev Biomed Eng. 20:171–210.

Roth BJ, Beaudoin DL. 2003. Approximate analytical solutions of the bidomain equations for electrical stimulation of cardiac tissue with curving fibers. Phys Rev E. 67, 051925.

Sachse FB. 2004. Computational cardiology: modeling of anatomy, electrophysiology, and mechanics. Berlin: Springer Verlag.

Skouibine K, Trayanova N, Moore P. 2000. A numerically efficient model for simulation of defibrillation in an active bidomain sheet of myocardium. Math Biosci. 166:85–100.

Sundnes J, Lines GT, Tveito A. 2005. An operator splitting method for solving the bidomain equations coupled to a volume conductor model for the torso. Math Biosci. 194:233–248.

Trayanova N. 2001. Concepts of ventricular defibrillation. Philos Trans Royal Soc London A. 359:1327–1337.

Trayanova N. 2006. Defibrillation of heart: insights into mechanisms from modelling studies. Exp Physiol. 91:323–337.

Tung L. 1978. A bidomain model for describing ischaemic myocardial dc potentials. PhD thesis, Massachusetts Institute of Technology.

Vigmond E, Aguel F, Trayanova N. 2002. Computational techniques for solving the bidomain equations in three dimensions. Biomed Eng IEEE Trans. 49:1260–1269.

Vigmond EJ, Hughes M, Plank G, Leon LJ. 2003. Computational tools for modeling electrical activity in cardiac tissue. J Electrocardiol. 36:69–74.

Vigmond E, dos Santos RW, Prassl A, Deo M, Plank G. 2008. Solvers for the cardiac bidomain equations. Progress Biophys Mol Biol. 96:3–18.

Zaret BL, Moser M, Cohen LS. 1992. Yale university school of medicine heart book. New York: William Morrow & Co.